How chemical defects influence the charging of nanoporous carbon supercapacitors

Romain Dupuis, Pierre-Louis Valdenaire, Roland Pellenq, Katerina Ioannidou

PNAS RESEARCH ARTICLE | ENGINEERING

How chemical defects influence the charging of nanoporous carbon supercapacitors

Romain Dupuis[a,b,c,d,1], Pierre-Louis Valdenaire[d,2], Roland J.-M. Pellenq[d,e], and Katerina Ioannidou[c,d,1]

Edited by Alexis Bell, University of California, Berkeley, CA; received December 3, 2021; accepted February 5, 2022

Ion desolvation and confinement are key physical processes in porous carbon-based supercapacitors undergoing charging and discharging cycles. We investigate electrolyte interactions between polarized porous carbon with subnanometer pore sizes and aqueous sodium chloride electrolyte, using molecular dynamics. Inspired by recent first-principles calculations, we develop a scheme accounting for chemical defects in electrodes where only the non-sp2 carbons species carry an extra negative charge (on the anode) and an extra positive charge (on the cathode) due to voltage polarization. This drives electrolyte species (ions and solvent molecules; water, in this work) to adsorb at the electrode surface and in subnanometric pores upon polarization. First, we observe an asymmetrical desolvation process of sodium and chloride ions at the external surface of the electrodes. The ionic distribution at the external surface of the electrodes is consistent with the Debye–Hückel electric potential equation and empirical trends observed for nonporous electrodes. In a second stage, we demonstrate that the nanoporosity of the electrodes is filled with ions and scarce water molecules and contributes to about 20% of the overall capacitance. A fraction of desolvated ions are irreversibly trapped in the core of electrodes during discharge. While maintaining the overall electroneutrality of the simulation cell, we find that anodes and cathodes do not carry the same amount of ions at all time steps, leading to charge imbalance.

supercapacitors | nanoporous carbon | ionic adsorption | atomistic simulations | energy storage

Significance

Nanoporous carbon texture makes fundamental understanding of the electrochemical processes challenging. Based on density functional theory (DFT) results, the proposed atomistic approach takes into account topological and chemical defects of the electrodes and attributes to them a partial charge that depends on the applied voltage. Using a realistic carbon nanotexture, a model is developed to simulate the ionic charge both at the surface and in the subnanometric pores of the electrodes of a supercapacitor. Before entering the smallest pores, ions dehydrate at the external surface of the electrodes, leading to asymmetric adsorption behavior. Ions in subnanometric pores are mostly fully dehydrated. The simulated capacitance is in qualitative agreement with experiments. Part of these ions remain irreversibly trapped upon discharge.

Understanding ions in nanoconfinement is the key element to get the fundamental physical basis of electrochemical energy storage underlying modern electrochemistry devices like batteries and supercapacitors (1, 2). In particular, fundamental understanding of the ionic adsorption processes and confinement inside nanoporous carbon electrodes is essential for predicting and improving the capacitance (3) or deionization efficiency of carbon-based devices (4, 5). Recent in situ X-ray (6) and neutron scattering (7) have shown that subnanometric pores of carbon electrodes enhance the ionic adsorption and its overall capacitance performance (8). In fact, if the pores are of the same size as electrolyte ions, high capacitances (leading to the term supercapacitor) have been observed that do not follow existing theories and empirical trends (9–12).

The term electrical double-layer (EDL) capacitor comes from the classical picture of nonporous electrodes that accumulate oppositely charged ions at their vicinity upon voltage polarization in a mean-field dielectric continuum description of the solvent populated with point charged ions at a given concentration. This picture, although very popular, obviously does not hold for porous electrodes with subnanometric pores. In particular, the mean-field Gouy–Chapman–Stern description of an EDL fails in high molar concentrations and for pore sizes smaller than a few nanometers (typically, 4 nm for carbon substrates) (13, 14). EDL predictions usually rely on the Poisson–Boltzmann theory and modified versions such as Debye–Hückel (15, 16) and Donnan models (17). More recent approaches based on thermodynamics theory for heterogeneous ionic fluids allow taking into account ionic size and, hence, ionic position correlations (18). Recently, this statistical physics description of an EDL theoretical prediction was extended to include time dependence and study the dynamics of the ionic charging process of a planar electrode (19).

Presently, there is no theory capable of solving the electrostatics problem for ions confined in the nanopores of a disordered porous carbon material commonly used in electrochemical devices. Nowadays, atomistic simulation techniques implement statistical physics methods that are able to describe both the intrinsic textural disorder of porous carbon materials at the nanoscale and the movement of electrolyte species (solvent molecules and ions) in their pores under operational functioning conditions of a supercapacitor device (i.e., under polarization) (20–23).

There are currently two main approaches to describe atomic systems under polarization, the constant voltage (CV) and the constant charge (CC) methods. 1) The CV approach

Author contributions: R.J.-M.P. and K.I. designed research; R.D., P.-L.V., R.J.-M.P., and K.I. performed research; R.D. and P.-L.V. analyzed data; and R.D., P.-L.V., R.J.-M.P., and K.I. wrote the paper.

The authors declare no competing interest.

This article is a PNAS Direct Submission.

[1]To whom correspondence may be addressed. Email: romain.dupuis@umontpellier.fr or aikaterini.ioannidou@umontpellier.fr.

[2]Deceased September 5, 2021.

This article contains supporting information online at https://www.pnas.org/lookup/suppl/doi:10.1073/pnas.2121945119/-/DCSupplemental.

Published April 19, 2022.

assumes a perfectly conducting substrate and, hence, accumulating/depleting charges only on the atoms at the pore and external surfaces with no regards to the intrinsically defective nature of porous carbons (Fig. 1*A*). Applied to porous carbon materials, the CV approach thus assumes that all carbon atoms are in the sp2 hybridization state, that is, conducting electrons. The main assumption of the CV method is, therefore, the metallic approximation—the electrodes are considered ideal conductors with no localization of electric charge except at the material boundaries in contact with the electrolyte. In recent simulation works (10), pore surfaces are treated as an extension of the external electrode surface. It is important to indicate that the charging process of substrate atoms is in the order of femtoseconds, while ion diffusion occurs at the scale of nanoseconds (24, 25). Thus, upon polarization, the charges on the solid matrix species attract ions first. Once equilibrium is reached, thermal agitation of adsorbed ions can induce (in a CV description) charge fluctuation on electrode atoms that, in turn, can redistribute ions in their vicinity. This is the main advantage of the CV approach; its main drawback is that it ignores charge localization due to chemical heterogeneity. As a result, within the CV approach, ion docking is only observed at the external surfaces of the electrodes or in large nanopores, the subnanopores being found not to participate in the capacitance, in sharp contrast to the experiment of activated carbon-based supercapacitors (Fig. 1*B*) (3).

2) The standard CC approach gives all substrate atoms the same fixed charge. The main drawback of the CC approach is that substrate charges are not allowed to fluctuate upon ion docking. Thus, this method only simulates the initial ion docking dynamics before charge self-regulation takes place. In the literature, it was reported that the CC approach may lead to an unphysical temperature increase (26). In the supporting information, we give evidence that this issue might come from the configurational setup of the simulation cell with bouncing walls for ions in a rigid electrodes approximation. With a full periodic cell simulating a stack of immersed electrodes, using microcanocical molecular dynamics (MD) simulation under polarization, we found that the temperature was well tempered (after initial relaxation at 300 K). However, this leads to unphysical ion docking deep in the electrodes regardless of the pore size (Fig. 1*B*). In sum, both the standard CC and CV methods fail for different reasons and, hence, are not able to reliably simulate the adsorption of ions in subnanoporous polarized electrodes (Fig. 1 *A* and *B*).

Therefore, we modified the CC method guided by experimental and theoretical results showing the key role of chemical defects and subnanopores in the building up of the capacitance (3, 9, 27–33). With this method, there is no additional computational cost compared to classical MD–CC calculations. The local electrostatic field generated by the matrix defects (in the present work, non-sp2 carbon atoms and edge hydrogen species) drives ion adsorption on the electrode external surface as well as in the whole porosity including the subnanopores. Our electrodes have a porous carbon texture that is found to be realistic for charcoal and activated carbon as well as for mature kerogen (34, 35). It was obtained using hybrid reverse Monte Carlo (36) with a density around 1 g/cm^3. Note that our activated carbon texture contains subnanometric pores of 0.5 nm to 0.9 nm (Fig. 1*D*). This sharply contrasts with carbide-derived carbons (CDCs) (37) previously used in supercapacitor simulations that only contain pores above 1 nm.

We propose a chemically driven charge localization model (CDCL) that locates partial charges to defective species through the entire electrode, including species at the external or pore surface that are, by nature, defective. It takes advantage of both CC

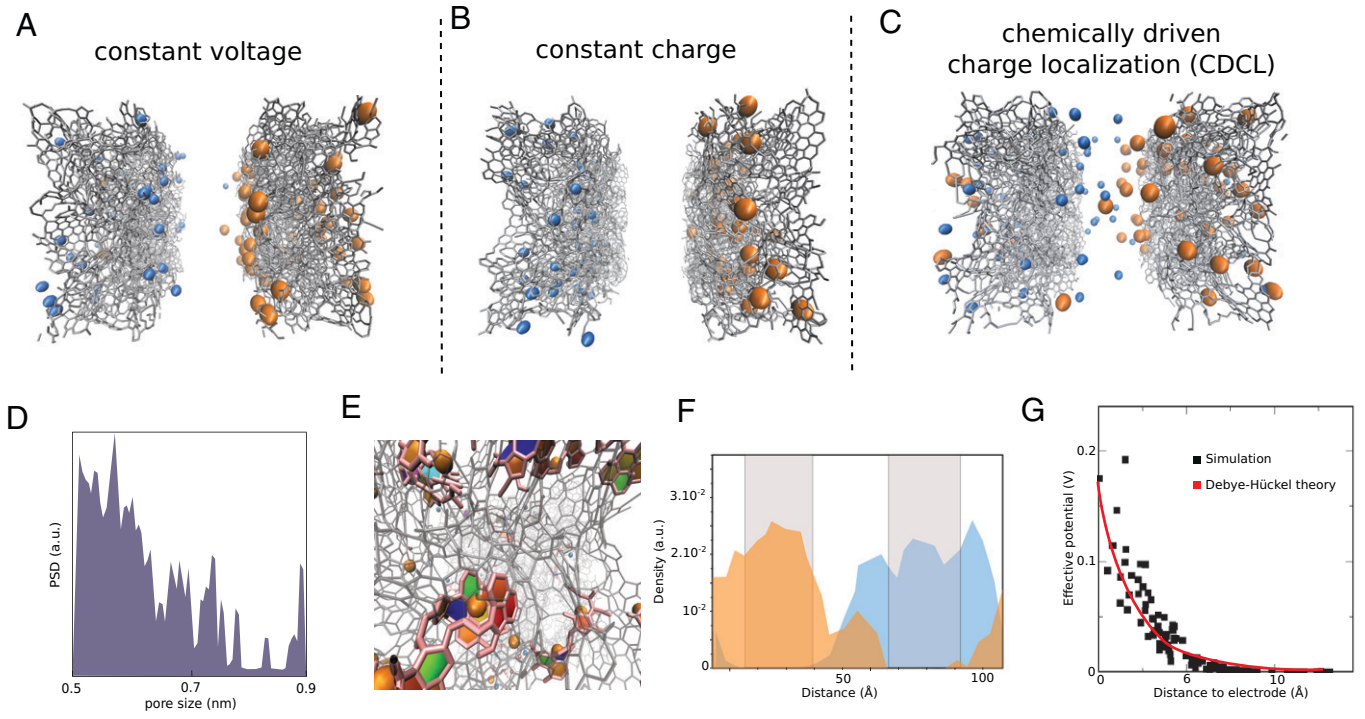

Fig. 1. (*A*–*C*) Snapshots of the system showing ionic adsorption in different polarization schemes upon steady state for the CC, the CV and the chemistry driven charge localization schemes respectively. (*D*) Pore size distribution of the electrodes. (*E*) structure of the local structure of the porous carbon electrode near adsorption sites. Colored surfaces are guides for the eyes to emphasizing the texture of the pores near the docked-ions. (*F*) density of Na (in blue) and Cl (in orange) for Δ_q = 0.02 e (1 V) along the simulation cell axis, the two gray bands correspond to the electrodes position and thickness. (*G*) Calculation of the effective electrical potential acting on the ions in the solution for Δ_q = 0.02 e (1 V). Effective potential acting on the ions in the simulation cell (in black). Due to the roughness, the position of the surface has to be defined arbitrarily, which has been done using the position of the most forward carbon atom of the electrode. Fit obtained using the Debye-Hückel formula (in red). The charge distribution follows a Debye-Hückel law due to the screening of the solution.

and CV methods while correcting their main drawbacks, opening the path for modeling the adsorption of ions in subnanoporous defective electrodes, including the role of doping of elements as such as N, S, F, etc.

We demonstrate that, using MD simulations with a nonreactive force field (38, 39) at 300 K, the CDCL approach unravels many subnanometric features underlying the physics of ion docking in the charged electrodes, ranging from the differentiated desolvation mechanism of cations with respect to anions to their asymmetric adsorption/desorption mechanism inside the nanopores. The pore size distribution shows a maximum at 0.5 nm to 0.6 nm (Fig. 1*D*). Sodium and chloride ions can only dock as single bare ions (i.e., unsolvated) in those pores. The electrodes are separated by 30 Å on both sides. The system is periodic in all directions, and it is initially prepared with 6,100 water molecules and 60 sodium and 60 chloride ions in the interelectrodes regions, corresponding to a salt concentration of 0.67 mol/L (see *Methods*). As shown in Fig. 1*E*, the texture of the electrode near the ions contains defects (incomplete rings or rings with five members). Fig. 1*F* shows the ion density after polarization, and we can observe ion docking inside the porous electrodes.

Results and Discussion

In view of the limitations identified for the CC and the CV method, we have chosen to develop the CDCL approach guided by the chemical attributes of the electrodes. Our electrodes are made of 70% sp2 carbon atoms, that is, having three carbon neighbors as immediate neighbors with a typical angle between consecutive carbon atoms of around 120°. The other 30% of carbon atoms can be considered as defects where charges are localized (an increase of partial charge for anode atoms, a decrease for cathode species) (40) (see density functional theory (DFT) calculations in *SI Appendix*).

Upon polarization, DFT calculations show that excess charges in absolute value are localized on the defects or in their vicinity (30). Therefore, the CDCL scheme for the attribution of additional charges consists in applying a Δ_q value to the non-sp2 carbon atoms while attributing a null charge to sp2 carbon atoms. The sp2 character is hereafter determined based on the C–C–C angle between three consecutive carbon atoms (*SI Appendix*). For the sake of simplicity, we assume the following linear formula for the excess charge estimate:

$$\begin{aligned}\Delta_q &= \Delta_{q,max} * (|(\Theta - \Theta_{max})|/10) \forall \Theta \\ &\in [\Theta_{max} - 10, \Theta_{max} + 10] \\ \Delta_q &= \Delta_{q,max} \forall \Theta \notin [\Theta_{max} - 10, \Theta_{max} + 10],\end{aligned} \quad [1]$$

where Θ_{max} is the value of the C–C–C angle in a perfect sp2 matrix (equal to 120°), and $\Delta_{q,max}$ is the maximum excess charge (positive for the anode and negative for the cathode), whose magnitude depends on the applied voltage. We calculated that a value of $\pm\Delta_{q,max}$ = 0.0337 e gives an excess/deficit average charge on the anode/electrode of Δ_q equals ±0.02 e. In order to compare our results with results obtained with the CV method, we have calculated a conversion factor by computing the average charge attributed to the electrode atoms in the CV method. If we apply 1 V, the average excess/deficit charge is ±0.02 e per carbon atom on the anode/cathode, respectively, which gives a voltage conversion factor of 0.02. In the CDCL approach, carbon defective species have a nominative charge that reflects their local chemical environment and is, in absolute value, proportional to the departure from the perfect sp2 state (Eq. **1**) and the applied voltage.

Recent CV atomistic simulations of CDC carbon-based porous structures have shown that solvated ions are adsorbed in pores above 1 nm in size; no fully dehydrated ions have been observed, implying that the subnanopores are still empty, in agreement with what we observe in our CV simulations (41). As demonstrated here below, it is important to note that the CDCL approach is the only method that is able to predict, at the same time, the adsorption of fully dehydrated ions inside the subnanopores (less than 1 nm; Fig. 1*C*), and partially or fully hydrated ions on the external surface or in any other kind of larger pores. All confinement environments were experimentally found to contribute to the overall capacitance of EDL devices (2).

First, we investigate the adsorption of ions on the external surface of the electrodes. The excess charge imposed additional Coulombic forces on the ions of the system. The effective voltage acting on the ions has been computed by extracting the Coulombic forces on the ions with and without electric field at the initial time of the simulation. The charge distribution, in Fig. 1*G*, shows that ions close to the external surface of the electrodes are the ones experiencing larger attraction forces, due to the applied voltage compared to ions in bulk electrolyte away from the electrode surface. Since it is related to a Coulombic term, the force experienced by the ions is proportional to Δ_q (Eq. **1**). The evolution of the effective potential depends on the characteristics of the electrolyte solution and the screening effect. Using the Debye–Hückel formula (42), we can compare the Debye length obtained from the simulation and that for a solution with a uniform ion distribution for an ionic concentration of 0.67 mol $\cdot L^{-1}$ (corresponding to the salt concentration in the interelectrode void), with a dielectric constant of 80 (43). The agreement between the simulation and the Debye–Hückel expression for the electric potential at the external surface of the anode is remarkably good and gives a Debye length of around 0.2 nm to 0.3 nm, in quantitative agreement with the Debye length obtained for this electrolyte type and concentration (43).

The number of effective ions adsorbed on and in both porous electrodes is related to the capacitance of the system. The capacitance has been calculated and is reported on Fig. 2*A* for each simulation with different Δ_q (the estimation of voltage is given from the aforementioned conversion). There is a threshold at low voltage above which ions are being adsorbed on the external surface of the electrodes (approximately Δ_q = 0.0025 e, corresponding to 0.125 V). For larger polarization voltages, the amount of ions incorporated in the electrodes increases quasi-linearly until it reaches the maximum; hence, the capacitance exhibits a peak shown in Fig. 2*A* in agreement with the recent theoretical and simulation work of Verkholyak et al. (44). Note that, at voltages above about 1.8 V, we consider that the simulation is probably unrealistic, since we do not consider water splitting that happens at these voltages (45). The capacitance is in agreement with the typical measured capacitance of activated carbons (around 100 F/g with a specific surface area at around 500 m^2/g for our carbon texture) (46). The maximum capacitance we find, of about 20 $\mu F/cm^2$, is in agreement with experimental values (2, 9, 10). Comparing the results obtained with the CV and the CDCL on Fig. 2*A*, we can estimate that the contribution of the subnanopores to the capacitance is about 20%, meaning that the supercapacitor made of subnanoporous electrodes remains mostly a standard EDL device with respect to aqueous electrolytes.

Due to the ionic docking in the subnanometric pores, the capacitance estimated from the CDCL method is larger than the one obtained with the CV method (dots, Fig. 2*A*). There is a positive correlation between the capacitance and the specific surface area as measured with BET experiments (47). In fact, the

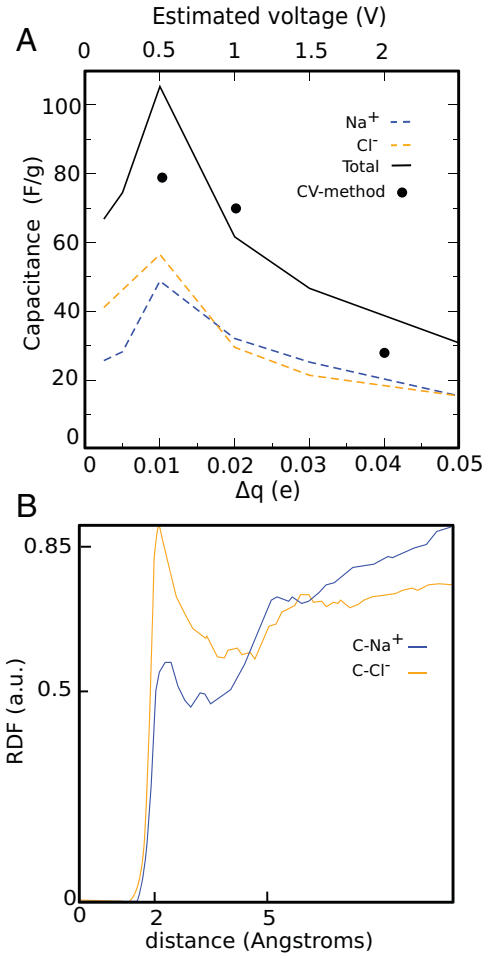

Fig. 2. (*A*) Capacitance due to sodium and chloride ions adsorbed inside and onto the electrodes at steady state with a maximum additional charge Δ_q (the added/subtracted charge is maximal on defective (non-sp2) sites). Note that the carbon atoms at the vicinity of the pores are not necessarily the non-sp2 carbons. The x-axis represents the excess of charge on each carbon atom of the positive electrode with respect to Δ_q. The dots correspond to the calculated value with the CV method. The simulated capacitance value is in the ball park of experimental values (100 F/g) for supercapacitors based on porous carbons with specific surface area around 500 m^2/g (which is the value of our simulated porous carbon) (*B*) Radial distribution functions for C-Na and C-Cl distances at steady state for Δ_q = 0.01 e.

large value of the specific surface area reflects both the amount of subnanopores and chemical defects on the carbon backbone. Chloride and sodium contribute differently to the capacitance (orange and blue dashed lines, Fig. 2*A*). The adsorption sites are different due to the ionic size, as shown by the radial distribution function in Fig. 2*B*. This leads to an asymmetric loading and charge-imbalanced electrodes, which is a direct consequence of the ion docking into the subnanometric pores (while the simulation cell overall charge remains neutral at all times in the simulation). The capacitance being the sum of the charges divided by the voltage, the peak can be explained with the less and less efficient ion docking upon voltage increase; this will be discussed hereafter.

In more detail, Fig. 3 *A* and *B* shows the number of adsorbed ions on the surface and inside the subnanopores of the electrodes during polarization simulations, and the total ionic loading during charge and discharge simulations with Δ_q = 0.01 e (Movie S1). At the voltage corresponding to the maximum capacitance, the total adsorption is larger for Cl^- than Na^+. Comparing Fig. 3 *A* and *B*, one can see that Na^+ is mostly adsorbed at the external surface, whereas Cl^- is equally adsorbed inside and at the external surface of the electrodes. We observe that half of the sodium ions are adsorbed; the rest remain in the solution in between the electrodes. Similarly, 2/3 of the chloride ions are adsorbed, and 1/3 remain in the electrolyte solution.

Fig. 3*C* shows the number of adsorbed ions 1) on the surface, 2) inside the nanopores, and 3) in total for different polarizations. Cl^- ions are partially adsorbed on the surface and inside the electrode nanopores following a monotonous increase until Δ_q = 0.01 e (0.5 V), and then the number of adsorbed ions reaches a plateau. Na^+ is adsorbed in larger quantity than Cl^- at voltages larger than Δ_q = 0.01 e (0.5 V). Interestingly, as the voltage increases, we observe a transition from an external surface adsorption only (from Δ_q = 0.0025 e to Δ_q = 0.01 e) to a dual inside-pore docking/surface adsorption for the sodium ions above Δ_q = 0.01 e (0.5 V). This is due to the fact that surface adsorption involves hydrated ions, whereas inside-pore docking involves bare ions. Low voltages do not provide enough energy to loosen the hydration shell of Na^+, leading to external surface adsorption of hydrated ions (2).

The process of ion adsorption in nanopores is accompanied by a change in the solvation shell of the ions. In bulk water, sodium ions have a first solvation shell made of approximately six water molecules (48), which is also observed in our simulations before charging the electrodes. An ion and its first-layer hydration shell are about 0.7 nm in diameter and, therefore, can only access the largest pores in our system.

Fig. 3*D* shows the evolution of the hydration shells of the adsorbed Na^+ and Cl^- ions together with the total number of adsorbed ions at Δ_q = 0.01 e (0.5 V). The adsorbed Na^+ ions are surrounded, on average, by four or five water molecules, whereas the Cl^- ions carry two or three water molecules. All adsorbed ions have lost their hydration shell either partially or totally, when adsorbed on the surface of the electrodes, or their whole hydration shell when entering the subnanopores. Fig. 3*E* shows the hydration number of Cl^- ions before adsorption and after adsorption inside the nanopores. The hydration shell becomes loose at the surface, and then the ions can enter either bare or with, at most, one water molecule in the subnanopores. Note that we observed the formation of anion–cation ionic pairs only in the solution outside of the electrodes.

Focusing now on the role of water in porous electrodes at full saturation, we observed that, in polarized electrodes, few water molecules adsorb in the pores of the electrodes (49). Fifteen percent or less of the total number water molecules are inside the two electrodes. The carbon structure is rather hydrophobic, as indicated by the radial distribution functions (shown in *SI Appendix*), the shortest C-water distance being about 3.5 Å.

Corrected for the effective accessible pore volume, the subnanopores are just large enough to accommodate one bare ion (diameter for sodium and chloride equals 0.1 nm and 0.18 nm, respectively), in agreement with the conclusions of Simon and Gogotsi (2). While the electrodes are being charged, the density of water inside the electrodes slightly increases. This indicates that the adsorption of ions into the carbon electrodes makes the structure less hydrophobic in a fashion similar to the way the clay interlayer void is hydrophilic only because of the presence of cations compensating the overall clay layer negative charge. The clay basal planes per se are rather hydrophobic, as they carry no OH surface groups immediately in contact with adsorbed water; the ions act as a water pump inside a polarized porous carbons or in between clay layers charged through isomorphic substitutions (50).

In summary, chloride and sodium ions in water are behaving differently upon the working conditions of a supercapacitor (51). Chloride species appear to be more mobile than sodium ions that are likely to get trapped in their tighter hydration cage (52). The

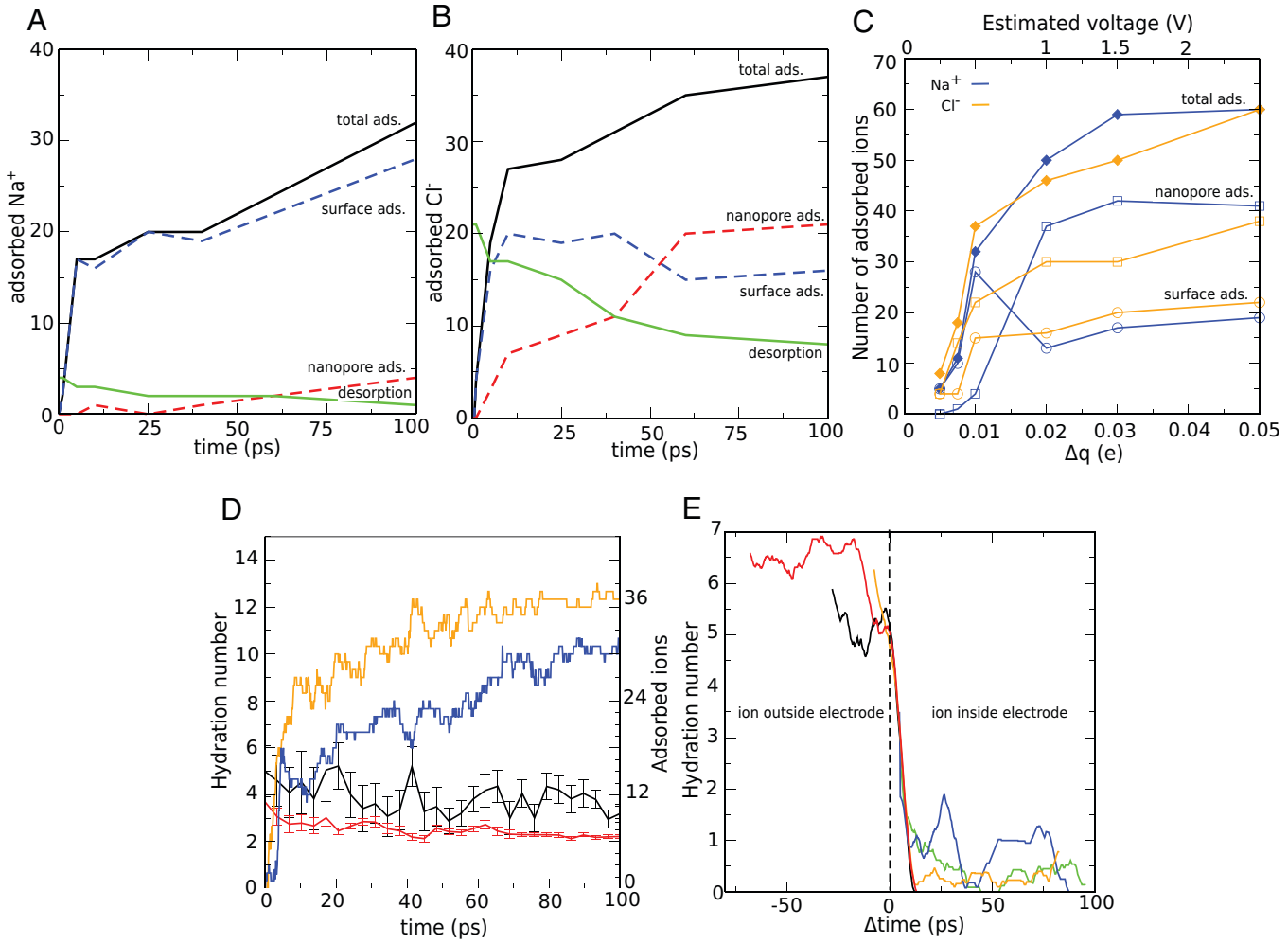

Fig. 3. (*A*) Evolution of the number of sodium ions in the electrode during the loading, adsorbed in the pore network (blue) or on the surface of the electrode (red) while imposing a voltage corresponding to a Δ_q = 0.01 e (0.5 V) (total in black) and during unloading (in green) for Δ_q = 0. To determine the adsorption, a cutoff of 4.0 Å and 5.0 Å have been used for Na-C and Cl-C distances respectively, corresponding to the first minimum in the radial distribution functions. (*B*) Evolution of the number of chloride ions in the electrode. (*C*) Number of (blue) sodium ions and (orange) chloride ions adsorbed (diamond) in total, (squares) inside the electrodes, (circles) at the surface. (*D*) Evolution of the hydration number during the adsorption around Na (black) and Cl (red) ions and number of ions adsorbed inside the electrodes at Δ_q = 0.01 e (0.5 V). Error bars correspond to the SD. Evolution of the quantity of adsorbed Na (blue) and Cl (orange). (*E*) Hydration number of several ions versus Δ time (each color corresponds to a different Na^+ ion), where Δ time is the time difference to the moment where the ion enters into the electrode. The values reported are the running average over 100 steps.

mobility of chloride over sodium ions is also confirmed by faster adsorption inside the carbon nanopores at lower voltage (Fig. 3 *A* and *B*).

Regarding the desorption process, the ions that are adsorbed deep in the core of the electrode will more likely remain trapped upon discharge. At voltage set back to zero, about 10% of the formerly docked Na^+ ions (about 3% of the total number of cations) and 30% of the adsorbed Cl^- (about 10% of the total number of anions) are still trapped inside the electrodes (after 1 ns of unloading, 2 Na^+ and 6 Cl^- are inside the electrodes; *SI Appendix*). Note that desorption, which is simulated under a null voltage, takes place over a longer time than ion docking (Fig. 3 *A* and *B*). The trapped ions may not participate in the current unloading cycle, but they could move to a nearby pore during the cycling and become again available for storage. The trapped ions upon depolarization are compatible with the hysteretic behavior observed in the supercapacitor current-voltage (I-V) curve. More specifically, the ions that are being desorbed at zero voltage are only the ions that have an easy path to exit the porous material. Other ions, that are in small pores or in tortuous porous network, are not easily extracted from the media. Being a smaller ion, Na^+ is often trapped more deeply in the porous network at larger voltages. Three adsorption/desorption cycles have been performed in this work, and we have observed that, after the first cycle, the amount of ions irreversibly docked inside the electrode nanoporosity remains constant.

Conclusion

We propose an approach to describe the charge and discharge process in subnanoporous carbon-made electrodes, in a supercapacitor setting, that we call CDCL. Despite its mean-field character, the CDCL approach is an improvement of the current standard methods to simulate charged devices at the atomic scale, namely the CC and the CV methods that are ineffective to correctly describe ionic docking in subnanopores. Informed from DFT calculations, the CDCL method consists in localizing charges on defective non-sp2 carbon sites, including chemical or topological defects. By contrast to the standard methods, this allows simulating both adsorption on the electrodes' external surfaces and in subnanopore docking.

Applied to a realistic texture of nanoporous carbon, we could unravel the fundamental processes underlying the capacitive effect of a subnanoporous carbon-based supercapacitor device in

operation. We show, in particular, that subnanometric pores constitute about 20% of the capacitance of such a device using a standard aqueous electrolyte. The simulated value of the capacitance of about 100 F/g (or 20 $\mu F/cm^2$) is in good agreement with the experimental values measured on activated carbon-based supercapacitors. In more detail, we show that the docking of ions in pores is preceded by an asymmetrical desolvation in the vicinity of the external pore surface. The ion adsorption density profile on the electrodes' external surfaces is in agreement with the Debye–Hückel theory with a Debye length of 0.2 nm to 0.3 nm. The desolvation process is actually different for sodium and for chloride ions, as the hydration shell of sodium is tighter than that of chloride. Once ions are desolvated, they can access nanopores, subnanopores being mostly populated with bare ions in agreement with in situ X-ray experiments (6). Due to the difference in their ionic size, the docking mechanism of sodium and chloride ions leads to imbalanced electrode charging. Upon discharge, we found that a significant amount of ions (10% of the cations and 30% of the anions) remains trapped in the subnanopores due to the pore network tortuosity right after the first charge that is compatible with the typical I-V curve of supercapacitors.

The current CDCL method allows exploration of how doping with elements such as N, S, etc., influences ion adsorption and in-pore docking (53). Furthermore, the current CDCL method could be coupled with a CV approach in order to take into account the variation of the substrate defects charge upon ionic thermal movement. This will allow studying the aging of the electrodes texture upon charge–discharge cycling.

Methods

A supercapacitor composed by porous carbon layers (of 22-Å thickness), separated with a water solution containing electrolytes, has been simulated with a fully atomistic approach. The electrodes have been generated using a liquid quench MD method (54) using the reactive force field ReaxFF (55) to obtain a microporous carbon containing hydrogen (0.3 H/C). The charges due to defects in the carbon structure are compensated by H atoms. This structure has been relaxed at 293 K and 1 atm, then cut in half in order to add a phase of bulk water replacing the other half. The cut leads to unstable atoms at the interface due to broken bonds. Thus, we performed a relaxation with an MD run at a higher temperature (1,500 K) to force water molecules to react with the unstable carbon atoms, stabilize the structure, and diffuse within the structure. Then, we have duplicated the system one time toward the orthogonal direction of the cut surface. Each electrode contains 5,440 atoms. It has a connected pore network and a density of 1.45 $g \cdot cm^{-3}$.

In order to study the charge of the capacitor with ions, we have built a model in which pure water solution has been enriched with 60 Na^+ and 60 Cl^- ions. We have investigated the adsorption of the ions in the porous carbon structure that has been described previously. Since ReaxFF is not well suited for simulating systems with electric fields, the potential used for the charge and discharge simulations is the Condensed-phase Optimized Molecular Potentials for Atomistic Simulation Studies force field (38, 39) to describe the electrodes–water interactions, and the SPC/E (extended simple point charge model) (56) potential, to describe water molecule interactions, which is well known for its good description of polar liquids. The interactions cutoff has been set to 12 Å. In this work, considering the complexity of the electrodes and therefore of finding a relevant force field to simulate the motion of the atoms of the electrodes, the electrodes were kept rigid. This is an approximation that could slightly influence the quantity of ions that can be adsorbed (in a flexible system, one can imagine that the pores will slightly adapt to the presence of ions). In further studies, the use of reactive force fields such as ReaxFF should be considered in order to assess the stability of the structure and the durability of the pore network due to the ion adsorption. Since such a reactive potential relies on the calculation of charges at each step of the dynamics, the CDCL method should be implemented as a postcalculation to add the charge excess/deficit after the electronegativity equalization method algorithm.

Ewald summation has been used for the long-range interactions. The particle-particle particle-mesh solver (PPPM) scheme, which is well suited for large systems (in this work, over 30,000 atoms), as implemented in LAMMPS (57) has been used with a threshold on the forces of 10^{-4}. Periodic boundary conditions have been imposed on the simulation cell. The electrodes are symmetrical, and the simulation cell is electroneutral.

For the dynamics, we have used a time step of 0.2 fs, in agreement with the frequency of the O–H stretching modes in water. The system has been thermostated using Nosé–Hoover thermostats. Before adding the electric field, the system has been equilibrated for 300 ps at 300 K. As discussed in *SI Appendix*, we have not observed any increase of temperature under the electric field, contrary to the results published in a recent work by Merlet et al. (26) that the authors attribute to a macroscopic dipole moment, which is an artifact of the simulation.

Data Availability. The data supporting the findings of this study are available within the article and its supplementary material.

ACKNOWLEDGMENTS. R.D., P.-L.V., and K.I. have been supported from CNRS Momentum Grant Cement-Nanocarbon Composites: Structural SuperCapacitors for Autonomous Buildings. Computations have been performed on the Grand équipement national de calcul intensif/Centre Informatique National de l'Enseignement Supérieur clusters within Project A0090911009.

Author affiliations: [a]Insitut Européen des Membranes, CNRS, ENSCM, Université de Montpellier, 34090 Montpellier, France; [b]Institute Charles Gerhard Montpellier, CNRS, ENSCM, Université de Montpellier, 34090 Montpellier, France; [c]Laboratoire de Mécanique et Génie Civil, CNRS Université de Montpellier, 34090 Montpellier, France; [d]MIT/CNRS/Aix-Marseille University Joint Laboratory "MultiScale Materials Science for Energy and Environment," Cambridge, MA 02139; and [e]International Research Laboratory, Epigenetics, Data & Politics CNRS and George Washington University, Washington, DC 20037

1. S. Chu, A. Majumdar, Opportunities and challenges for a sustainable energy future. *Nature* **488**, 294–303 (2012).
2. P. Simon, Y. Gogotsi, Materials for electrochemical capacitors. *Nat. Mater.* **7**, 845–854 (2008).
3. F. Béguin, V. Presser, A. Balducci, E. Frackowiak, Carbons and electrolytes for advanced supercapacitors. *Adv. Mater.* **26**, 2219–2251, 2283 (2014).
4. S. Porada, R. Zhao, A. van der Wal, V. Presser, P. Biesheuvel, Review on the science and technology of water desalination by capacitive deionization. *Prog. Mater. Sci.* **58**, 1388–1442 (2013).
5. M. E. Suss *et al.*, Water desalination via capacitive deionization: What is it and what can we expect from it? *Energy Environ. Sci.* **8**, 2296–2319 (2015).
6. C. Prehal *et al.*, Quantification of ion confinement and desolvation in nanoporous carbon supercapacitors with modelling and in situ X-ray scattering. *Nat. Energy* **2**, 16215 (2017).
7. S. Boukhalfa *et al.*, In situ small angle neutron scattering revealing ion sorption in microporous carbon electrical double layer capacitors. *ACS Nano* **8**, 2495–2503 (2014).
8. R. Futamura *et al.*, Partial breaking of the Coulombic ordering of ionic liquids confined in carbon nanopores. *Nat. Mater.* **16**, 1225–1232 (2017).
9. J. Chmiola *et al.*, Anomalous increase in carbon capacitance at pore sizes less than 1 nanometer. *Science* **313**, 1760–1763 (2006).
10. C. Merlet *et al.*, Highly confined ions store charge more efficiently in supercapacitors. *Nat. Commun.* **4**, 2701 (2013).
11. S. Kondrat, P. Wu, R. Qiao, A. A. Kornyshev, Accelerating charging dynamics in subnanometre pores. *Nat. Mater.* **13**, 387–393 (2014).
12. H. Shao, Y. C. Wu, Z. Lin, P. L. Taberna, P. Simon, Nanoporous carbon for electrochemical capacitive energy storage. *Chem. Soc. Rev.* **49**, 3005–3039 (2020).
13. M. Müllier, B. Kastening, The double layer of activated carbon electrodes: Part 1. The contribution of ions in the pores. *J. Electroanal. Chem. (Lausanne)* **374**, 149–158 (1994).
14. M. Salanne *et al.*, Efficient storage mechanisms for building better supercapacitors. *Nat. Energy* **1**, 16070 (2016).
15. N. Boon, R. van Roij, 'Blue energy' from ion adsorption and electrode charging in sea and river water. *Mol. Phys.* **109**, 1229–1241 (2011).
16. R. A. Rica, R. Ziano, D. Salerno, F. Mantegazza, D. Brogioli, Thermodynamic relation between voltage-concentration dependence and salt adsorption in electrochemical cells. *Phys. Rev. Lett.* **109**, 156103 (2012).
17. P. M. Biesheuvel, R. Zhao, S. Porada, A. van der Wal, Theory of membrane capacitive deionization including the effect of the electrode pore space. *J. Colloid Interface Sci.* **360**, 239–248 (2011).
18. J. P. de Souza, M. Z. Bazant, Continuum theory of electrostatic correlations at charged surfaces. *J. Phys. Chem. C* **124**, 11414–11421 (2020).
19. C. Lian, S. Zhao, H. Liu, J. Wu, Time-dependent density functional theory for the charging kinetics of electric double layer containing room-temperature ionic liquids. *J. Chem. Phys.* **145**, 204707 (2016).
20. L. Yang, B. H. Fishbine, A. Migliori, L. R. Pratt, Molecular simulation of electric double-layer capacitors based on carbon nanotube forests. *J. Am. Chem. Soc.* **131**, 12373–12376 (2009).
21. H. Liu, C. J. Jameson, S. Murad, Molecular dynamics simulation of ion selectivity process in nanopores. *Mol. Simul.* **34**, 169–175 (2008).

22. R. K. Kalluri, D. Konatham, A. Striolo, Aqueous NaCl solutions within charged carbon-slit pores: Partition coefficients and density distributions from molecular dynamics simulations. *J. Phys. Chem. C* **115**, 13786–13795 (2011).
23. G. Feng, P. T. Cummings, Supercapacitor capacitance exhibits oscillatory behavior as a function of nanopore size. *J. Phys. Chem. Lett.* **2**, 2859–2864 (2011).
24. C. Hauf, M. Woerner, T. Elsaesser, Macroscopic electric polarization and microscopic electron dynamics: Quantitative insight from femtosecond X-ray diffraction. *Phys. Rev. B* **98**, 054306 (2018).
25. T. Sun *et al.*, Rapid electron transfer by the carbon matrix in natural pyrogenic carbon. *Nat. Commun.* **8**, 14873 (2017).
26. C. Merlet *et al.*, Simulating supercapacitors: Can we model electrodes as constant charge surfaces? *J. Phys. Chem. Lett.* **4**, 264–268 (2013).
27. S. A. Evlashin *et al.*, Role of nitrogen and oxygen in capacitance formation of carbon nanowalls. *J. Phys. Chem. Lett.* **11**, 4859–4865 (2020).
28. G. Hartmann, G. S. Hwang, First-principles description of electrocatalytic characteristics of graphene-like materials. *J. Chem. Phys.* **153**, 214704 (2020).
29. T. Hussain, E. Olsson, K. Alhameedi, Q. Cai, A. Karton, Functionalized two-dimensional nanoporous graphene as efficient global anode materials for Li-, Na-, K-, Mg-, and Ca-ion batteries. *J. Phys. Chem. C* **124**, 9734–9745 (2020).
30. A. Maslechko, T. Verstraelen, T. S. van Erp, E. Riccardi, Multiscale partial charge estimation on graphene for neutral, doped and charged flakes. *Phys. Chem. Chem. Phys.* **20**, 20678–20687 (2018).
31. D. I. Abouelamaiem *et al.*, New insights into the electrochemical behaviour of porous carbon electrodes for supercapacitors. *J. Energy Storage* **19**, 337–347 (2018).
32. M. E. Suss *et al.*, Impedance-based study of capacitive porous carbon electrodes with hierarchical and bimodal porosity. *J. Power Sources* **241**, 266–273 (2013).
33. J. Segalini, B. Daffos, P. Taberna, Y. Gogotsi, P. Simon, Qualitative electrochemical impedance spectroscopy study of ion transport into sub-nanometer carbon pores in electrochemical double layer capacitor electrodes. *Electrochim. Acta* **55**, 7489–7494 (2010).
34. J. Pikunic *et al.*, Structural modeling of porous carbons: Constrained reverse Monte Carlo method. *Langmuir* **19**, 8565–8582 (2003).
35. S. K. Jain, R. J. M. Pellenq, J. P. Pikunic, K. E. Gubbins, Molecular modeling of porous carbons using the hybrid reverse Monte Carlo method. *Langmuir* **22**, 9942–9948 (2006).
36. C. Bousige, A. Boţan, F. J. Ulm, R. J. M. Pellenq, B. Coasne, Optimized molecular reconstruction procedure combining hybrid reverse Monte Carlo and molecular dynamics. *J. Chem. Phys.* **142**, 114112 (2015).
37. C. Prehal *et al.*, A carbon nanopore model to quantify structure and kinetics of ion electrosorption with in situ small-angle X-ray scattering. *Phys. Chem. Chem. Phys.* **19**, 15549–15561 (2017).
38. H. Sun, COMPASS: An ab initio force-field optimized for condensed-phase applications overview with details on alkane and benzene compounds. *J. Phys. Chem. B* **102**, 7338–7364 (1998).
39. M. J. McQuaid, H. Sun, D. Rigby, Development and validation of COMPASS force field parameters for molecules with aliphatic azide chains. *J. Comput. Chem.* **25**, 61–71 (2004).
40. A. B. Bogeat, Understanding and tuning the electrical conductivity of activated carbon: A state-of-the-art review. *Crit. Rev. Solid State Mater. Sci.* **46**, 1–37 (2019).
41. N. Ganfoud *et al.*, Effect of the carbon microporous structure on the capacitance of aqueous supercapacitors. *Energy Storage Mater.* **21**, 190–195 (2019).
42. C. G. Gray, P. J. Stiles, Nonlinear electrostatics: The Poisson–Boltzmann equation. *Eur. J. Phys.* **39**, 053002 (2018).
43. A. M. Smith, A. A. Lee, S. Perkin, The electrostatic screening length in concentrated electrolytes increases with concentration. *J. Phys. Chem. Lett.* **7**, 2157–2163 (2016).
44. T. Verkholyak, A. Kuzmak, S. Kondrat, Capacitive energy storage in single-file pores: Exactly solvable models and simulations. *J. Chem. Phys.* **155**, 174112 (2021).
45. X. Li *et al.*, Water splitting: From electrode to green energy system. *Nano Micro Lett.* **12**, 131 (2020).
46. F. Barzegar *et al.*, Investigation of different aqueous electrolytes on the electrochemical performance of activated carbon-based supercapacitors. *RSC Advances* **5**, 107482–107487 (2015).
47. E. Frackowiak, "Electrode materials with pseudocapacitive properties" in *Supercapacitors: Materials, Systems, and Applications*, F. Béguin, E. Frackowiak, Eds. (John Wiley, 2013), pp. 207–237.
48. D. G. Levitt, S. R. Elias, J. M. Hautman, Number of water molecules coupled to the transport of sodium, potassium and hydrogen ions via gramicidin, nonactin or valinomycin. *Biochim. Biophys. Acta* **512**, 436–451 (1978).
49. J. K. Brennan, K. T. Thomson, K. E. Gubbins, Adsorption of water in activated carbons: Effects of pore blocking and connectivity. *Langmuir* **18**, 5438–5447 (2002).
50. D. Ebrahimi, R. J. M. Pellenq, A. J. Whittle, Nanoscale elastic properties of montmorillonite upon water adsorption. *Langmuir* **28**, 16855–16863 (2012).
51. G. Cassone, F. Creazzo, P. V. Giaquinta, F. Saija, A. Marco Saitta, Ab initio molecular dynamics study of an aqueous NaCl solution under an electric field. *Phys. Chem. Chem. Phys.* **18**, 23164–23173 (2016).
52. R. Mancinelli, A. Botti, F. Bruni, M. A. Ricci, A. K. Soper, Hydration of sodium, potassium, and chloride ions in solution and the concept of structure maker/breaker. *J. Phys. Chem. B* **111**, 13570–13577 (2007).
53. L. Liu, P. L. Taberna, B. Dunn, P. Simon, Future directions for electrochemical capacitors. *ACS Energy Lett.* **6**, 4311–4316 (2021).
54. R. Ranganathan, S. Rokkam, T. Desai, P. Keblinski, Generation of amorphous carbon models using liquid quench method: A reactive molecular dynamics study. *Carbon* **113**, 87–99 (2017).
55. A. C. T. van Duin, S. Dasgupta, F. Lorant, W. A. Goddard, Reaxff: A reactive force field for hydrocarbons. *J. Phys. Chem. A* **105**, 9396–9409 (2001).
56. H. J. C. Berendsen, J. R. Grigera, T. P. Straatsma, The missing term in effective pair potentials. *J. Phys. Chem.* **91**, 6269–6271 (1987).
57. S. Plimpton, Fast parallel algorithms for short-range molecular dynamics. *J. Comput. Phys.* **117**, 1–19 (1995).